

Muon capture on nuclei: random phase approximation evaluation versus data for $6 \leq Z \leq 94$ nuclei

N. T. Zinner

*Institute for Physics and Astronomy
University of Aarhus, DK-8000 Aarhus C, Denmark*

K. Langanke

*GSI Darmstadt and Technische Universität Darmstadt, D-64220 Darmstadt, Germany
and P. Vogel*

*W. K. Kellogg Radiation Laboratory, 106-38
California Institute of Technology, Pasadena, California 91125, USA*

We use the random phase approximation to systematically describe the total muon capture rates on all nuclei where they have been measured. We reproduce the experimental values on these nuclei to better than 15% accuracy using the free nucleon weak form factors and residual interactions with a mild A dependency. The isospin dependence and the effects associated with shell closures are fairly well reproduced as well. However, the calculated rates for the same residual interactions would be significantly lower than the data if the in-medium quenching of the axial-vector coupling constant is employed to other than the true Gamow-Teller amplitudes. Our calculation thus suggests that no quenching is needed in the description of semileptonic weak processes involving higher multipole transitions and momentum transfer $\sim m_\mu$, with obvious importance to analogous weak processes.

PACS numbers: 24.30.Cz, 23.40.-s, 23.40.Hc

I. INTRODUCTION

The capture of a negative muon from the atomic $1s$ orbit,

$$\mu^- + (Z, N) \rightarrow \nu_\mu + (Z - 1, N + 1)^* \quad (1)$$

is a semileptonic weak process that has been studied for a long time (see, e.g., the recent review [1] or the earlier one by Walecka [2] and the classic by Mukhopadhyay [3] and the earlier references therein). The total capture rate has been measured for many stable nuclei; in some cases the capture rates on separated isotopes have been also determined [4].

The nuclear response in muon capture is governed by the momentum transfer of the order of the muon mass. The phase space and the nuclear response favor lower nuclear excitation energies, thus the nuclear states in the giant resonance region dominate. Since the experimental data are quite accurate, and the theoretical techniques of evaluating the nuclear response in the relevant regime are well developed, it is worthwhile to see to what extent the capture rates are understood globally. Such a comparison may be viewed as a general test of our ability to describe semileptonic weak charged-current reactions with $q \sim m_\mu$ over a large range of nuclei, where q is the momentum transfer and $m_\mu = 105.6$ MeV is the muon mass.

The present work represents a first fully comprehensive theoretical evaluation of the total muon capture rate over the full range of nuclei where the experimental data are available. Previously, the muon capture rates for selected nuclei encompassing, however, a broad range of atomic charges, were calculated in Ref. [5]. That paper was devoted mostly to the description of the radiative muon capture, and the total muon

capture rates were a byproduct with only a limited agreement with the data. More along the lines of the present approach, Ref. [6] and [7] used a Hatree-Fock random phase approximation method and obtained good agreement with experiment, however only for a limited selection of nuclei. The local Fermi gas model was used successfully for the evaluation of the muon capture rate in selected nuclei in Ref. [8], and more recently in Ref. [9].

The present work is an extension of previous papers devoted to this issue [10, 11]. In Ref. [10] the capture rates for ^{12}C , ^{16}O and ^{40}Ca were evaluated using the continuum random phase approximation, and a very good agreement with the total rate was obtained. However, the residual interaction employed in [10] was adjusted to describe other observables in the cases of ^{12}C and ^{16}O . Moreover, it was necessary to quench the Gamow-Teller like (GT) partial capture rate leading to the 1^+ ground state of ^{12}B . In the later Ref. [11] heavier nuclei with $N > Z$, $^{44,48}\text{Ca}$, ^{56}Fe , ^{90}Zr , and ^{208}Pb were also included with a similar success. In Ref. [11] it has also been shown that for the calculation of muon capture rates the standard random phase approximation (SRPA) is essentially equivalent to the more computationally demanding continuum random phase approximation. Thus, the SRPA method is also used in the present study. In Ref. [12] the SRPA approach has been used to study the muon capture rates to a long chain of calcium and tin isotopes.

One of the important issues when evaluating the response of nuclei to weak probes of relatively low energies is the problem of quenching of the corresponding strength. The evidence for quenching comes primarily from the analysis of the beta decay of the (*sd*) shell [13] as well as (*p, f*) shell [14] nuclei. In addition, the interpretation of the forward angle (*p, n*) and (*n, p*) charge-exchange reactions [15, 16, 17] leads to the same conclusion. All such evidence, so far, is restricted to the GT strength and relatively low excitation energies. A convenient and customary way to account for this quenching is to use an ‘effective’ axial-vector coupling constant g_A , reducing it from its nominal value of $g_A = 1.26$ to $g_A \sim 1$.

The evaluation of the muon capture rate, reported here, suggests that the quenching of g_A is not needed to describe these data. (That conclusion was already reached in Refs.[10, 11].) As stressed above, the mean excitation energy in muon capture is in the region of giant resonances of about 15 MeV (slowly decreasing with A or Z), and the GT-like operators contribute very little in heavier nuclei where the neutrons and protons are in different oscillator shells. In lighter nuclei, for N and Z less than 40, the GT strength contributes, and is concentrated at low energy. Thus, in agreement with the evidence mentioned above, we quench this, and only this, part of the transition strength by a common factor $(0.8)^2 = 0.64$ [13].

The present work, and the evaluation of the muon capture in general, makes it possible to extend the study of quenching to higher multipoles, and correspondingly to higher nuclear excitation energies. Such processes, typically, depend primarily on the positions of the corresponding giant resonances and on the overall strength. Our conclusions, therefore, show that the SRPA method involving correlated particle-hole excitations, is capable of describing the inclusive semileptonic processes with momentum transfer q of order $\sim m_\mu$ quite well. This is an important conclusion, applicable to a variety of practically important subjects, e.g. detection of supernova neutrinos or evaluation of the nuclear matrix elements for neutrinoless double beta decay.

The challenge of evaluating the muon capture rate in a wide variety of nuclei made it necessary to include several effects that were not usually included in analogous calculations. Since we needed to describe the bound muon in the $1s$ orbit well, we went beyond the usual calculation of the muon density at the site of the nucleus. First, we solved the Dirac equation in the field of the finite size nucleus numerically. We then used its wave function, taking into account that it is not constant between the origin and the nuclear surface. For high Z values the muon is relativistic, and the ‘small’ $p_{1/2}$ component of its wave function is nonnegligible. As explained below, we used here (for the first time) the additional transition matrix elements associated with that component.

Since our goal is to describe muon capture in all nuclei (except the very light ones) we have to describe, at least crudely, effects associated with the partial filling of the single-particle subshells for nuclei that do

not have magic numbers of protons and/or neutrons. As described in the next section, we describe these effect by taking into account the smearing of the proton and neutron Fermi levels caused by pairing and deformation. It appears that this simplified treatment of complicated correlations, including those caused by deformation, is sufficient for our purpose.

II. METHOD AND PARAMETERS

In this calculation we have used the standard RPA model to describe the nuclear excitations. In a previous work ([11]) this model was shown to be just as good as the computationally more involved continuum RPA. As residual interaction we use the phenomenological Landau-Migdal force. For low mass nuclei the parameters for the force were taken from Ref. [18]. This choice was shown to be accurate in [10]. For muon capture the most important term in the Landau-Migdal force is the spin-isospin coupling constant g' . In [18] the value $g'=0.7$ is recommended, however, in a recent review [19] $g'=0.96$ is used for heavy nuclei. To accommodate this variation, we use an interpolation formula with a mild A dependency:

$$g' = c_1 + c_2 A^{1/3} \quad (2)$$

where the constants c_1 and c_2 are fitted to yield $g'=0.7$ in ^{16}O and $g'=0.96$ in ^{208}Pb . We note that the change in the total capture rate in going from $g'=0.7$ to $g'=0.96$ is less than 10%.

To get a basis of single-particle states we diagonalize a Woods-Saxon potential (WSP) in a harmonic oscillator basis of more than 8 major shells, thus enabling us to always have an excess of $2\hbar\omega$ of valence space above the Fermi level for both protons and neutrons. As parameters of the WSP we use $R_0 = 1.2 * A^{1/3}$ fm for the radius and $a = 0.53$ fm for the diffuseness. The spin-orbit term is given as the derivative of the WSP times a strength V_{so} . Here we have simply used a fixed value of $V_{so} = -8.95$ through-out, initially checking that other choices did not significantly effect the total capture rate. To find the overall strength of the WSP, we fixed the last proton and neutron particle energies to experimentally known masses. More specifically, for a nucleus (A,Z) we found the energy of the last proton level from the proton separation energy S_p in (A,Z) . For the last neutron level we used the neutron separation energy S_n , but this time in the daughter $(A,Z-1)$.

In order to be able to handle open-shell nuclei we have previously used a simple scheme where partial occupancies was treated by multiplying the open level matrix elements by occupation numbers corresponding to an independent particle model [20]. In this work we have attempted to improve on this treatment by solving the standard BCS equations to determine the occupation numbers. Following Ref.[22] the occupation probabilities are given by

$$v_k^2 = \frac{1}{2} \left(1 - \frac{\epsilon_k - \mu}{\sqrt{\Delta^2 + (\epsilon_k - \mu)^2}} \right) \quad (3)$$

where ϵ_k are the single-particle energies and the chemical potential μ is fixed by the condition $N = \sum_k v_k^2 (2j_k + 1)$. The pairing gap Δ is obtained by the procedure descibed in Ref. [23].

The formalism used to evaluate the total muon capture rate is that of Ref. [2]. As mentioned in the Introduction, we treat the muon wavefunction by solving the Dirac equation in the extended charge of the nucleus, which is assumed to be of the Woods-Saxon form with the same paramteres as above. For nuclei with large values of Z , the atomic binding energy becomes a significant fraction of the muon rest mass and the small component of the Dirac bi-spinor may not be negligible in this range. We therefore explicitly include all terms containing both large and small components in our transition operators. An outline of the complications arising from this is given in the Appendix.

III. RESULTS

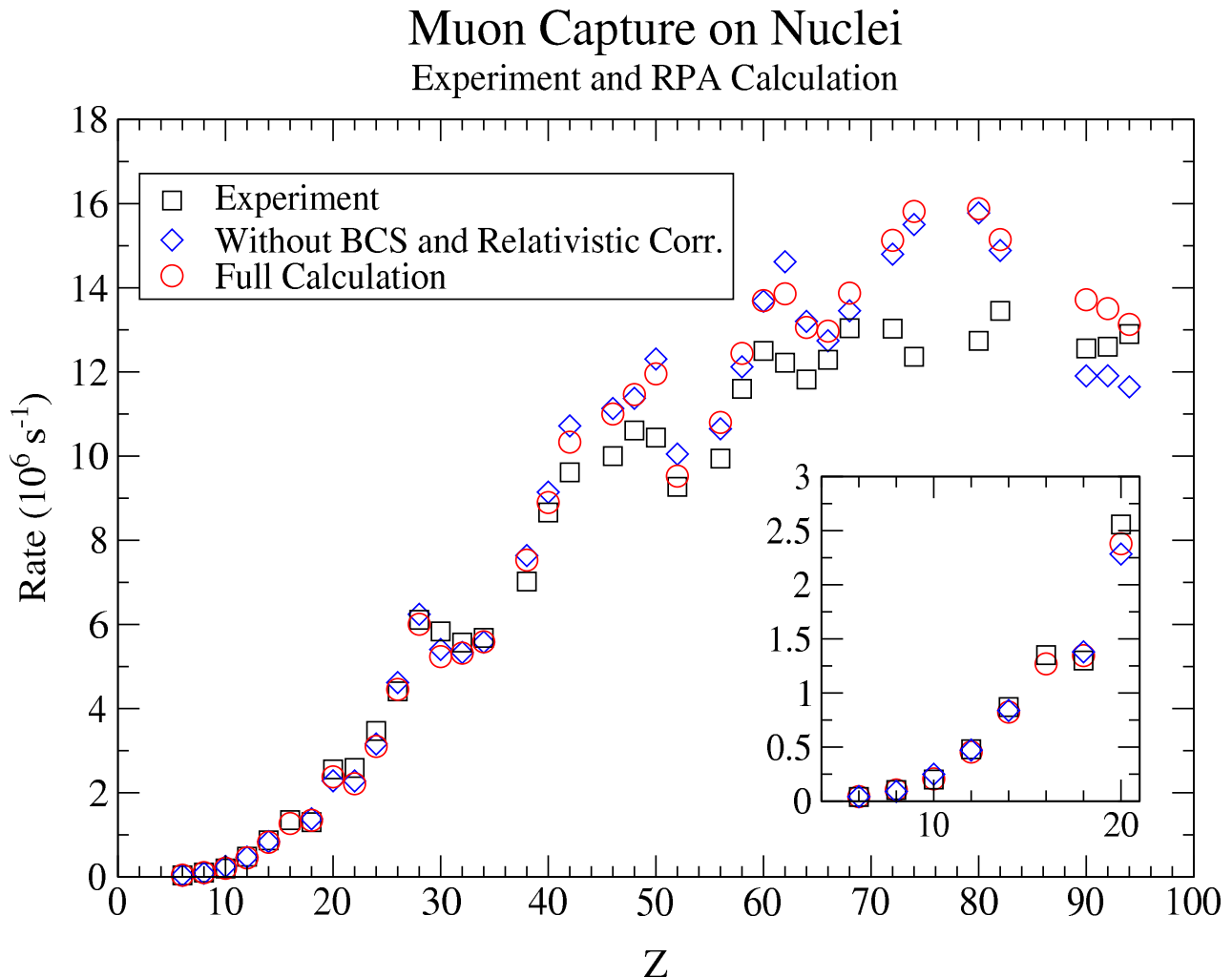


FIG. 1: (color online) Comparison between the measured total muon capture rates [4] denoted by squares \square , the calculated rates with all corrections (empty circles \circ), and the calculated rates without the BCS and relativistic corrections (diamonds \diamond). The insert, in larger scale, shows the same results for light nuclei. When the measurements are for the natural abundance of a given element, the calculation represent the corresponding combination of the individual isotopes.

Our calculated total muon capture rates for all nuclei for which measured values exist are shown in Figure 1. One sees that the overall agreement is quite good. With the exceptions at $Z = 74$ and 80 the calculations reproduce the experimental values to 15% or better. In Figure 2 we provide a ratio plot where the degree of agreement is better seen. In addition, in Table I we collect all our calculated capture rates, including the results for individual isotopes.

In Fig. 1 the total capture rates are also compared with values obtained from calculations where the BCS occupancy and the relativistic corrections are turned off. From this comparison it is clear that these are only small corrections, providing justification for the calculation done in Ref. [10, 11, 20]. At low Z one especially notices the good reproduction of the distinct dips in the rates above the magic numbers $Z = 20$ and 28 . For $Z = 50$ the same trends is visible in both calculation and experiment, but the calculations

overshoot the experimental values somewhat. Just above $Z = 60$, where the $N = 82$ closed neutron shell comes into play, we also overestimate the capture rates. This continues into the region with $Z = 74$ and 80 , and also, to a lesser extent, to the doubly-magic nucleus ^{208}Pb . One should remember that some of the nuclei above $Z = 50$ and below $Z = 82$ are deformed and thus have different single-particle structures than the ones given by our spherical mean-field model, thus a perfect agreement should not be expected. The fact that the calculated values are again approaching experiment at Th, U and Pu is likely a consequence of the same dip after the magic shell closure that was seen at lower Z also (these trends were also noted in Ref. [21], see in particular figure 3 of that reference).

As stated above, we use the unquenched value for the axial-vector coupling constant for all multipole operators, except for the true Gamow-Teller transition. For most of the light- and medium-mass nuclei, $\lambda = 1^-$ (dipole-like) and $\lambda = 2^+$ (quadrupole-like) transitions dominate. However, for ^{208}Pb and the heavier nuclei, $\lambda = 1^+$ transitions contribute significantly to the total capture rate. For these nuclei, the neutron excess is already so large that, in the simple independent particle model, 2 major oscillator shells have to be overcome when changing a proton into a neutron in the muon capture process. Thus, for these excitations the $\lambda = 1^+$ multipole transition corresponds to a $2\hbar\omega$ mode and not to a $(0\hbar\omega)$ Gamow-Teller transition; the contribution of the latter to the rate in the heavy nuclei vanishes in our calculations. We have not renormalized the axial-vector coupling constant for such $2\hbar\omega$ 1^+ transitions, supported by the good agreement of the the calculated capture rates with the measured results for the heavy nuclei.

An important test of the ability of a nuclear structure model to reproduce the data is the dependence of the muon capture rate on the number of neutrons for a fixed nuclear charge Z . Typically, the rate decreases with increasing N (or A) as subsequently more neutron levels are getting blocked. This effect is incorporated into the well-known Primakoff parametrization by its $(N-Z)$ dependence [26]. As examples, table I include three isotope chains of nuclei (Ca, Cr, and Ni), where total capture rates for individual isotopes have been measured. One sees that the isotope dependence is well reproduced by our calculations. Analogous calculations were performed in Ref. [12, 27].

IV. CONCLUSION

The present analysis shows that the standard random phase approximation method is capable of describing quite well the total μ^- capture rates for essentially all stable nuclei. The dependence of the capture rate on the isospin, or neutron excess, the so-called Primakoff rule [26], is also fairly well, albeit not perfectly, reproduced. Our calculation even describes the rather subtle effects of shell closures when considering the dependence of the capture rate on Z and/or A . There is no indication of the need to apply any quenching to the operators responsible for the muon capture, in particular those involving single-particle transitions from one oscillator shell to another, i.e. other than those involving $0\hbar\omega$ spin and isospin changing operators.

Given the task of describing the capture in a variety of nuclei, including those with high charge Z and nuclei with unfilled shells, it became necessary to consider several effects that have not been typically included previously. One of them is a fully relativistic treatment of the muon bound state, including the effects associated with the ‘small’ $p_{1/2}$ component of its wave function. Another one is the effect of the smearing of the Fermi level (both for protons and neutrons) in nuclei that have nonmagic Z or N numbers. Even though the corresponding corrections are not very large, they contribute noticeably to the overall good agreement between the experimental data and our calculated values.

Our findings then can be used as guidance in the evaluation of a wide variety of semileptonic weak processes on nuclei with similar momentum transfer.

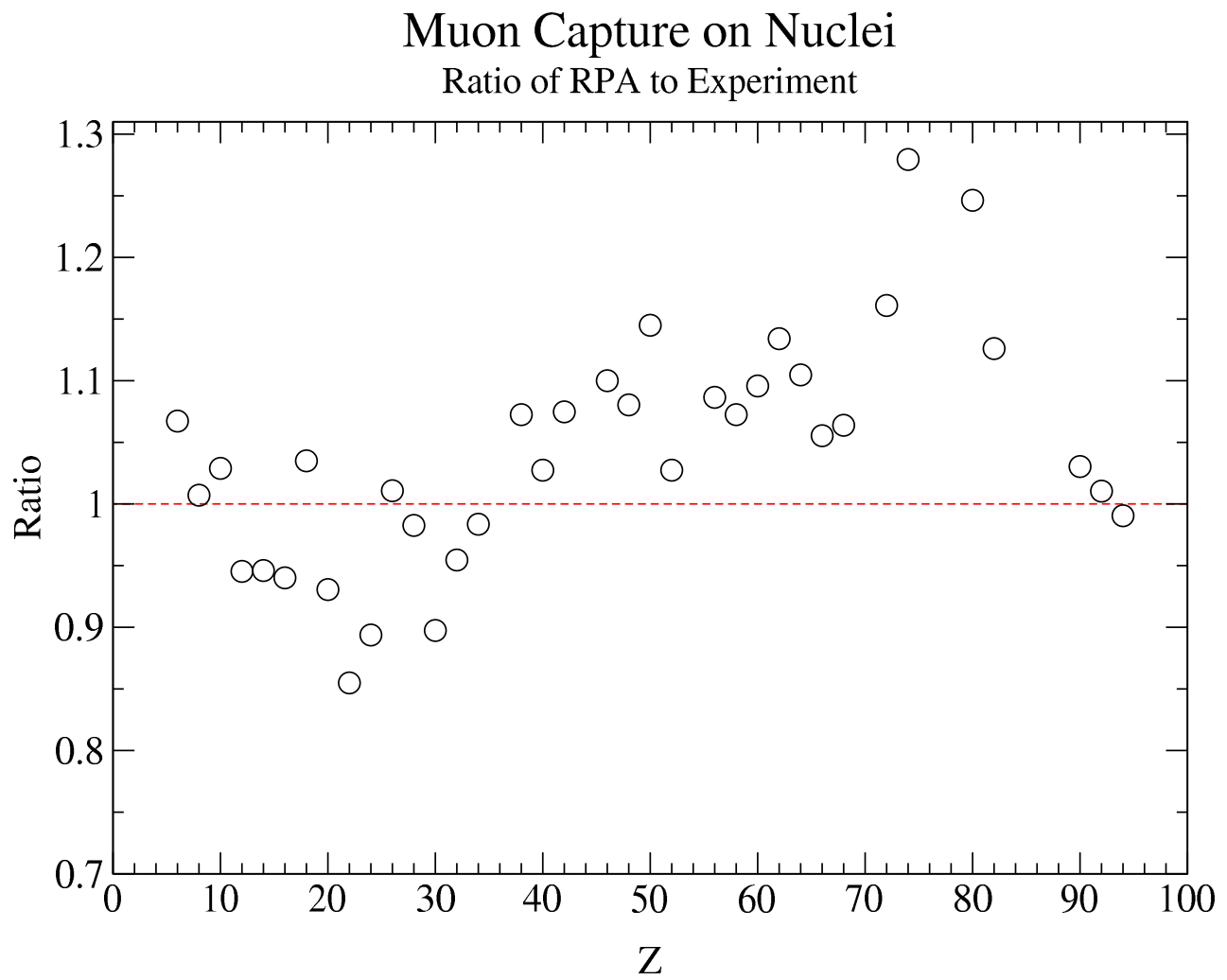


FIG. 2: (color online) Ratios of the calculated and measured total muon capture rates vs. the atomic number.

V. ACKNOWLEDGMENT

One of us (P.V.) gratefully acknowledges the hospitality at GSI, where part of this work was done.

VI. APPENDIX

In this appendix we give an outline of terms arising from the inclusion of the fully relativistic treatment of the bound muon wave function, i.e., of both the large and small components. The muon wavefunction we use has the form

$$\phi_{jm} = \begin{pmatrix} ig(r)\Omega_{jlm}(\hat{r}) \\ -f(r)\Omega_{jl'm}(\hat{r}) \end{pmatrix} \quad (4)$$

where the radial functions satisfy the equations

$$\frac{d}{dr} \begin{pmatrix} g \\ f \end{pmatrix} = \begin{pmatrix} -\frac{1+\kappa}{r} & E + m_\mu - V(r) \\ -E + m_\mu + V(r) & -\frac{1-\kappa}{r} \end{pmatrix} \begin{pmatrix} g \\ f \end{pmatrix}, \quad (5)$$

where $g(r), f(r)$ are the large and small components, respectively. Here

$$\kappa = \begin{cases} -(l+1) & , j = l + \frac{1}{2} \\ l & , j = l - \frac{1}{2} \end{cases} \quad (6)$$

and

$$\Omega_{j,l,m}(\hat{r}) = \sum_{m_l, m_s} (l, 1/2, j | m_l, m_s, m) Y_{l,m_l}(\hat{r}) \chi_{m_s} \quad (7)$$

These equations are entirely general and can be found in e.g. Ref. [28]. Since we assume that the muon is captured from the atomic 1s orbit we have $l = 0$ and $l' = 1$. Since l' is non-zero, we can no longer just multiply the wavefunction with the irreducible nuclear operators and obtain good total angular momentum. If the positive z-axis is chosen along the direction of the out-going neutrino then its wavefunction becomes

$$\psi = N \begin{pmatrix} \chi_- \\ -\chi_- \end{pmatrix} \exp(i\vec{p} \cdot \vec{x})$$

Here χ_- are the usual spin down Pauli two-spinors and N is a normalization given in [28]. This wavefunction makes the neutrino purely left-handed as the standard model prescribes.

The approach used in [2] neglects the small component in the muon wave function and expands the neutrino plane wave in multipoles. As the large component has $l = 0$, angular momentum coupling of the muon wave function and the multipole operators is quite straightforward. This is, however, no longer the case if the small component with orbital angular momentum $l = 1$ is considered, implying the need for a cumbersome recoupling of angular momenta to regain tensor operators that can be applied in the nuclear Hilbert space. This results in a more complicated expression for the weak Hamiltonian governing muon capture with several new terms. In the notation used in [2] the Hamiltonian with all terms from both

components can be written as

$$\begin{aligned}
\mathcal{H} = & \frac{2 G_F \cos \theta_C N^*}{\sqrt{2}} \left[\sum_{J=0}^{\infty} \sqrt{4\pi} [J] (-i)^J \{ i \delta_{m,-1/2} \left\{ \mathcal{M}'_{J,0} - \mathcal{L}'_{J,0} \right\} \right. \\
& + \alpha \left(J-1, J, m + \frac{1}{2} \right) \mathcal{T}_1 \left(J-1, J, m + \frac{1}{2} \right) \\
& + \alpha \left(J+1, J, m + \frac{1}{2} \right) \mathcal{T}_1 \left(J+1, J, m + \frac{1}{2} \right) \\
& - i \beta_+ (J, J, m) \mathcal{T}_2 (J, J, m + \frac{1}{2}) \\
& - i \beta_+ (J+1, J, m) \mathcal{T}_2 (J+1, J, m + \frac{1}{2}) \\
& - i \beta_+ (J+1, J+2, m) \mathcal{T}_2 (J+1, J+2, m + \frac{1}{2}) \\
& - i \beta_- (J-1, J-2, m) \mathcal{T}_3 (J-1, J-2, m + \frac{1}{2}) \\
& - i \beta_- (J-1, J, m) \mathcal{T}_3 (J-1, J, m + \frac{1}{2}) \\
& \left. - i \beta_- (J, J, m) \mathcal{T}_3 (J, J, m + \frac{1}{2}) \right\} \\
& + \sum_{J=1}^{\infty} \sqrt{4\pi} [J] (-i)^J \{ i \delta_{m,1/2} \left\{ \mathcal{J}'_{J,1}^{el} - \mathcal{J}'_{J,1}^{mag} \right\} \right. \\
& - \delta (J-1, J-1, m) \mathcal{T}_4 (J-1, J-1, m + \frac{1}{2}) \\
& - \delta (J-1, J-1, m) \mathcal{T}_4 (J-1, J-1, m + \frac{1}{2}) \\
& - \delta (J, J, m) \mathcal{T}_4 (J, J, m + \frac{1}{2}) \\
& - \delta (J, J+1, m) \mathcal{T}_4 (J, J+1, m + \frac{1}{2}) \\
& - \delta (J+1, J+1, m) \mathcal{T}_4 (J+1, J+1, m + \frac{1}{2}) \\
& + i \eta_+ (J, J, m) \mathcal{T}_2 (J, J, m + \frac{1}{2}) \\
& + i \eta_+ (J+1, J, m) \mathcal{T}_2 (J+1, J, m + \frac{1}{2}) \\
& + i \eta_+ (J+1, J+2, m) \mathcal{T}_2 (J+1, J+2, m + \frac{1}{2}) \\
& - i \eta_- (J-1, J, m) \mathcal{T}_3 (J-1, J, m + \frac{1}{2}) \\
& - i \eta_- (J, J, m) \mathcal{T}_3 (J, J, m + \frac{1}{2}) \\
& \left. - i \eta_- (J-1, J-2, m) \mathcal{T}_3 (J-1, J-2, m + \frac{1}{2}) \right\}]
\end{aligned}$$

Here we have defined the tensor operators in the nuclear Hilbert space as

$$\begin{aligned}
\mathcal{M}'_{J,M} &= \int d^3\vec{x} g(r) Y_{0,0} j_J(\kappa x) Y_{J,M} J_0 \\
\mathcal{L}'_{J,M} &= \frac{i}{\kappa} \int d^3\vec{x} g(r) Y_{0,0} \nabla (j_J(\kappa x) Y_{J,M}) J_0 \\
\mathcal{J}'_{J,M}{}^{mag} &= \int d^3\vec{x} g(r) Y_{0,0} j_J(\kappa x) \vec{\mathcal{Y}}_{J,J,1}^M \cdot \vec{J} \\
\mathcal{J}'_{J,M}{}^{el} &= \frac{1}{\kappa} \int d^3\vec{x} g(r) Y_{0,0} \nabla \wedge (j_J(\kappa x) \vec{\mathcal{Y}}_{J,J,1}^M) \cdot \vec{J} \\
\mathcal{T}_1(\gamma, \rho, \mu) &= \int d^3\vec{x} f(r) j_\rho(\kappa x) Y_{\gamma,\mu} J_0 \\
\mathcal{T}_2(\gamma, \rho, J, \mu) &= \int d^3\vec{x} f(r) j_{J+1}(\kappa x) \vec{\mathcal{Y}}_{\gamma,\rho,1}^\mu \cdot \vec{J} \\
\mathcal{T}_3(\gamma, \rho, J, \mu) &= \int d^3\vec{x} f(r) j_{J-1}(\kappa x) \vec{\mathcal{Y}}_{\gamma,\rho,1}^\mu \cdot \vec{J} \\
\mathcal{T}_4(\gamma, \rho, J, \mu) &= \int d^3\vec{x} f(r) j_J(\kappa x) \vec{\mathcal{Y}}_{\gamma,\rho,1}^\mu \cdot \vec{J},
\end{aligned}$$

where Y are the spherical harmonics and $\vec{\mathcal{Y}}$ are the vector harmonics. The first four operators are those involving the large component and are identical with the ones given in [2]. Their tensor character is (J, M) . The last four are new operators, i.e. they were ignored in [2], involving the small component of the muon wavefunction. Their tensor character is (γ, μ) . The other indices of the new operators identify terms which originate in the multipole expansion to produce the correct spherical Bessel function in the integrals. The constants appearing in the Hamiltonian above are given by the rather lengthy expressions

$$\begin{aligned}
\alpha(\gamma, \rho, m) &= \sqrt{\frac{3/2+m}{3}} \sqrt{\frac{3}{4\pi}} \frac{[\rho]}{[\gamma]} \langle \rho 1 \gamma | 000 \rangle \langle \rho 1 \gamma | 0 m + \frac{1}{2} m + \frac{1}{2} \rangle \\
\beta_+(\gamma, \rho, J, m) &= \sqrt{\frac{3/2+m}{3}} \sqrt{\frac{3}{4\pi}} \sqrt{J+1} [J+1] \langle 1 J + 1 \rho | 000 \rangle \\
&\quad \times \langle 1 J \gamma | m + \frac{1}{2} 0 m + \frac{1}{2} \rangle W(1 J + 1 \gamma 1; \rho J) \\
\beta_-(\gamma, \rho, J, m) &= \sqrt{\frac{3/2+m}{3}} \sqrt{\frac{3}{4\pi}} \sqrt{J} [J-1] \langle 1 J - 1 \rho | 000 \rangle \\
&\quad \times \langle 1 J \gamma | m + \frac{1}{2} 0 m + \frac{1}{2} \rangle W(1 J - 1 \gamma 1; \rho J) \\
\delta(\gamma, \rho, J, m) &= \sqrt{\frac{3/2-m}{3}} \sqrt{\frac{3}{4\pi}} [J]^2 \langle 1 J \rho | 000 \rangle \\
&\quad \times \langle 1 J \gamma | m - \frac{1}{2} 1 m + \frac{1}{2} \rangle W(1 J \gamma 1; \rho J) \\
\eta_+(\gamma, \rho, J, m) &= \sqrt{\frac{3/2-m}{3}} \sqrt{\frac{3}{4\pi}} \sqrt{J} [J+1] \langle 1 J + 1 \rho | 000 \rangle \\
&\quad \times \langle 1 J \gamma | m - \frac{1}{2} 1 m + \frac{1}{2} \rangle W(1 J + 1 \gamma 1; \rho J) \\
\eta_-(\gamma, \rho, J, m) &= \sqrt{\frac{3/2-m}{3}} \sqrt{\frac{3}{4\pi}} \sqrt{J+1} [J-1] \langle 1 J - 1 \rho | 000 \rangle \\
&\quad \times \langle 1 J \gamma | m - \frac{1}{2} 1 m + \frac{1}{2} \rangle W(1 J - 1 \gamma 1; \rho J)
\end{aligned}$$

Here we have repeatedly used the standard notation $[J] = \sqrt{2J+1}$. All conventions for the Clebsch-Gordan coefficients and W-symbols are those of [29].

In the derivation of the Hamiltonian given above we have used various selection rules for the Clebsch-Gordan coefficients and the W-symbols. Note that some of the terms vanish at low angular momenta, since

γ and ρ must be positive for any term to contribute. The quantity m in the above expressions corresponds to the spin projection of the muon. Since we consider unpolarized muons we must average over the two values $m = \pm 1/2$.

For completeness we list here the relevant nuclear currents for the muon capture process. These are

$$\begin{aligned}
\hat{\rho}_V(\vec{x}) &= G_E \sum_{j=1}^A \tau_+(j) \delta^{(3)}(\vec{x} - \vec{x}_j) \\
\hat{J}_V(\vec{x}) &= \frac{G_E}{2Mi} \sum_{j=1}^A \tau_+(j) \left[\delta^{(3)}(\vec{x} - \vec{x}_j) \vec{\nabla}_j - \overleftarrow{\nabla}_j \delta^{(3)}(\vec{x} - \vec{x}_j) \right] \\
&\quad + \frac{G_M}{2M} \vec{\nabla} \wedge \sum_{j=1}^A \tau_+(j) \vec{\sigma}(j) \delta^{(3)}(\vec{x} - \vec{x}_j) \\
\hat{\rho}_A &= \frac{G_A}{2Mi} \sum_{j=1}^A \tau_+(j) \vec{\sigma} \cdot \left[\delta^{(3)}(\vec{x} - \vec{x}_j) \vec{\nabla}_j - \overleftarrow{\nabla}_j \delta^{(3)}(\vec{x} - \vec{x}_j) \right] \\
&\quad + \frac{m_\mu G_P}{2M} \vec{\nabla} \cdot \sum_{j=1}^A \tau_+(j) \vec{\sigma}(j) \delta^{(3)}(\vec{x} - \vec{x}_j) \\
\hat{J}_A(\vec{x}) &= G_A \sum_{j=1}^A \tau_+(j) \vec{\sigma}(j) \delta^{(3)}(\vec{x} - \vec{x}_j)
\end{aligned}$$

here M is the nucleon mass, G_E and G_M are the Sachs nucleon form factors and G_A is the axial form factor. We note that the usual Fermi and Gamow-Teller transition operators are recovered in the $q \rightarrow 0$ limit as the following multipole components (see, e.g. [30])

$$\begin{aligned}
\mathcal{M}_{0,0} &= \frac{1}{\sqrt{4\pi}} G_V \sum_{j=1}^A \tau_+(j) \\
\mathcal{L}_{1,M} &= \frac{1}{\sqrt{2}} \mathcal{T}_{1,M}^{el} = \frac{i}{\sqrt{12\pi}} G_A \sum_{j=1}^A \tau_+(j) \sigma_{1,M}(j)
\end{aligned}$$

where G_V is the $q \rightarrow 0$ limit of the vector coupling form factor, which is often denoted by $F_1(0)$ in the literature.

To get the final expression for the total rate one must now evaluate the absolute squared matrix element of the Hamiltonian in the initial and final nuclear states and multiply it by the two-body phase space factor given in [2]. It is advantageous to group together the components with like tensor order to better control the interference of operators arising from the large and small components.

-
- [1] D. F. Measday, Phys. Rep. **354** (2001) 243
 - [2] J. D. Walecka in *Muon Physics II*, edited by V.W. Hughes and C. S. Wu (Academic Press, NY, 1975) p. 113.
 - [3] N. C. Mukhopadhyay, Phys. Rep. **30C**, 1 (1977).
 - [4] T. Suzuki, D. F. Measday, and J. P. Roalsvig, Phys. Rev. C **35**, 2212 (1987).
 - [5] H. W. Fearing and M. S. Welsh, Phys. Rev. C **46**, 2077 (1992).
 - [6] N. Auerbach and A. Klein, Nucl. Phys. **A422** 480 (1984)
 - [7] N. Auerbach, N. Van Giai and O. K. Vorov, Phys. Rev. C **56** R2368 (1997)
 - [8] H. C. Chiang, E. Oset and P. Fernández de Córdoba, Nucl. Phys. **A510** 591 (1990)
 - [9] J. Nieves, J. E. Amaro, and M. Valverde, Phys. Rev. C **70**, 055503 (2000); J. E. Amaro, C. Maieron, J. Nieves, and M. Valverde, Eur.Phys. J **A24**, 343 (2005).
 - [10] E. Kolbe, K. Langanke, and P. Vogel, Phys. Rev. C **50**, 2576 (1994).
 - [11] E. Kolbe, K. Langanke, and P. Vogel, Phys. Rev. C **62**, 055502 (2000).
 - [12] N. T. Zinner, K. Langanke, K. Riisager and E. Kolbe, Eur. Phys. J. **A17** (2003) 625
 - [13] B. H. Wildenthal, Prog. Part. Nucl. Phys. **11**, 5 (1984).
 - [14] E. Caurier, A. Poves, and A. P. Zuker, Phys. Rev. Lett, **74**, 1517 (1995).
 - [15] C. D. Goodman and S. B. Bloom, in *Spin excitation in nuclei*, F. Petrovich *et al.* eds., (Plenum, NY 1983); G. F. Bertsch and H. Esbensen, Rep. Prog. Phys. **50**, 607 (1987); O. Häusser *et al.*, Phys. Rev. C **43**, 230 (1991).
 - [16] K. Langanke, D.J. Dean, P.B. Radha, Y. Alhassid and S.E. Koonin, Phys. Rev. **C52** (1995) 718
 - [17] G. Martinez-Pinedo, A. Poves, E. Caurier and A.P. Zuker, Phys. Rev. **C53** (1996) R2602
 - [18] G. A. Rinker and J. Speth, Nucl. Phys. **A306**, 306 (1978).
 - [19] F. Grümmer and J. Speth, nucl-th/0603052.
 - [20] E. Kolbe, K. Langanke, and P. Vogel Nucl. Phys. **A652** 91 (1999).
 - [21] H. Hänscheid *et. al.*, Z. Phys. A - Atomic Nuclei **335** 1 (1990)
 - [22] A. Fetter and J. D. Walecka *Quantum Theory of Many-Particle Systems* (McGraw-Hill, San Francisco, 1971).
 - [23] A. Bohr and B. Mottelson *Nuclear Structure* Vol.I (W.A. Benjamin, Inc. 1969), pages 169-171.
 - [24] H. O. U. Fynbo *et. al.*, Nucl. Phys. **A724** 493 (2003).
 - [25] P. David *et. al.* Z. Phys. A - Atomic Nuclei **330** 397 (1988)
 - [26] H. Primakoff, Rev. Mod. Phys. **31**, 802 (1959).
 - [27] E. Kolbe, K. Langanke and K. Riisager, Eur. Phys. J. **A11** (2001) 25.
 - [28] W. Greiner: *Relativistic Wave Equations*, English Edition, Springer (1996).
 - [29] A. R. Edmonds: *Angular Momentum in Quantum Mechanics*, Princeton University Press (1957).
 - [30] J. D. Walecka: *Theoretical Nuclear and Subnuclear Physics*, 2nd edition, World Scientific, Singapore (2004).

Nuc	exp	calc	Nuc	exp	calc	Nuc	exp	calc
¹² C	0.039	0.042	¹⁶ O	0.103	0.104	¹⁸ O	0.088	0.089
²⁰ Ne	0.204	0.206	²⁴ Mg	0.484	0.454	²⁸ Si	0.871	0.823
³² S	1.352	1.269	⁴⁰ Ar	1.355	1.345	⁴⁰ Ca	2.557	2.379
⁴⁴ Ca	1.793	1.946	⁴⁸ Ca	1.214 ¹	1.455	⁴⁸ Ti	2.590	2.214
<i>nat</i> Cr	3.472	3.101	⁵⁰ Cr	3.825	3.451	⁵² Cr	3.452	3.085
⁵⁴ Cr	3.057	3.024	⁵⁶ Fe	4.411	4.457	<i>nat</i> Ni	5.932	6.004
⁵⁸ Ni	6.110	6.230	⁶⁰ Ni	5.560	5.563	⁶² Ni	4.720	4.939
<i>nat</i> Zn	5.834	5.235	⁶⁴ Zn		5.735	⁶⁶ Zn		4.976
⁶⁸ Zn		4.328	<i>nat</i> Ge	5.569	5.317	⁷⁰ Ge		5.948
⁷² Ge		5.311	⁷⁴ Ge		4.970	<i>nat</i> Se	5.681	5.588
⁷⁸ Se		6.023	⁸⁰ Se		5.485	⁸² Se		5.024
<i>nat</i> Sr	7.020	7.529	⁸⁶ Sr		8.225	⁸⁸ Sr	6.610	7.445
<i>nat</i> Zr	8.660	8.897	⁹⁰ Zr		8.974	⁹² Zr		9.254
⁹⁴ Zr		8.317	<i>nat</i> Mo	9.614	10.33	⁹² Mo		10.80
⁹⁴ Mo		11.01	⁹⁶ Mo		10.04	⁹⁸ Mo		9.153
<i>nat</i> Pd	10.00	11.00	¹⁰⁴ Pd		12.71	¹⁰⁶ Pd		11.44
¹⁰⁸ Pd		10.44	¹¹⁰ Pd		9.607	<i>nat</i> Cd	10.61	11.46
¹¹⁰ Cd		12.58	¹¹² Cd		11.51	¹¹⁴ Cd		11.21
¹¹⁶ Cd		10.44	<i>nat</i> Sn	10.44	11.95	¹¹⁶ Sn		13.08
¹¹⁸ Sn		12.35	¹²⁰ Sn		11.64	¹²² Sn		10.82
¹²⁴ Sn		10.15	<i>nat</i> Te	9.270	9.523	¹²⁶ Te		10.20
¹²⁸ Te		9.639	¹³⁰ Te		9.043	<i>nat</i> Ba	9.940	10.80
¹³⁶ Ba		11.45	¹³⁸ Ba		10.73	<i>nat</i> Ce	11.60	12.44
¹⁴⁰ Ce		12.38	¹⁴² Ce		12.95	<i>nat</i> Nd	12.50	13.70
¹⁴² Nd		13.67	¹⁴⁴ Nd		14.12	¹⁴⁶ Nd		13.15
<i>nat</i> Sm	12.22	13.86	¹⁴⁸ Sm		15.01	¹⁵² Sm		13.23
¹⁵⁴ Sm		12.08	<i>nat</i> Gd	11.82	13.06	¹⁵⁶ Gd		14.15
¹⁵⁸ Gd		13.06	¹⁶⁰ Gd		12.03	<i>nat</i> Dy	12.29	12.97
¹⁶² Dy		13.45	¹⁶⁴ Dy		12.54	<i>nat</i> Er	13.04	13.87
¹⁶⁶ Er		14.46	¹⁶⁸ Er		13.51	¹⁷⁰ Er		13.22
<i>nat</i> Hf	13.03	15.13	¹⁷⁸ Hf		15.44	¹⁸⁰ Hf		14.89
<i>nat</i> W	12.36	15.81	¹⁸² W		16.37	¹⁸⁴ W		15.79
¹⁸⁶ W		15.32	<i>nat</i> Hg	12.74	15.88	¹⁹⁸ Hg		17.17
²⁰⁰ Hg		16.29	²⁰² Hg		15.43	²⁰⁴ Hg		14.58
<i>nat</i> Pb	13.45	15.15	²⁰⁶ Pb		15.54	²⁰⁸ Pb		14.97
²³² Th	12.56	13.71	²³⁴ U	13.79	14.89	²³⁶ U	13.09 ²	14.17
²³⁸ U	12.57 ²	13.51	²⁴² Pu	12.90	13.13	²⁴⁴ Pu	12.40 ³	12.70

TABLE I: Calculated rates for natural elements and for the important individual isotopes. All rates are in the form $xx \times 10^6 \text{ s}^{-1}$. If the natural abundance has more than 90% of a given isotope then the Nuc column gives this particular isotope and the calculation is done for this nucleus only. Whenever a nucleus has the superscript *nat* the calculation is a weighted combination of all isotopes contributing more than 10% to the natural abundance. An empty experiment box means that the given isotope has not been measured. Natural abundance measurements appear in the box next to the most abundant isotope. Experimental data are from Ref. [4], where the original sources may be found. ¹ is taken from Ref. [24], ² is from Ref. [21] and ³ is from Ref. [25]